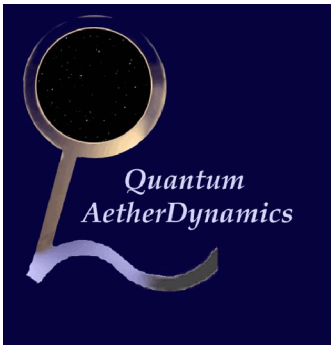


**Quantum AetherDynamics Institute (QADI)**

# Coherence-Window Quantization in Photoemission: Dual Electrostatic and Magnetic Gate Laws in QMU

David W. Thomson III
**Quantum AetherDynamics Institute (QADI)**, Alma, Illinois, USA
ORCID: 0000-0002-5830-5427

Version 1.0 – January 27, 2026

This article is published by the Quantum AetherDynamics Institute (QADI).

It develops the Aether Physics Model (APM)

**Abstract**

This note supplies a compact event-level quantization mechanism for the photoelectric effect in Quantum Measurement Units (QMU). A finite gate coherence window $\tau_g$ (dimensionless $\tau_g^* := \tau_g F_q$) converts a fixed-quantum photon-front cadence into an integer count $N(\nu^*)$ of coherently admissible quanta per emission event. The resulting "surplus law" produces (i) a sharp threshold set by an integer $N_0$ and (ii) a staircase post-threshold energy descriptor which, under ensemble averaging, approaches the familiar quasi-linear dependence on $\nu^*$ without requiring a continuously variable photon quantum. To keep the physics experimentally decidable, we introduce dual conjugate potential-like scalars $\varphi_e := \mathrm{enrg}_e/e^2$ and $\psi_e := \mathrm{enrg}_e/{e_{\mathrm{emax}}}^2$ that parameterize the same event energy in electrostatic and magnetic charge primitives identified with the emitted electron kinetic-energy descriptor in the zero-smear limit. Two competing gate laws are then stated: an electrostatic-primary coherence control ($\tau_g^*, N_0$ governed mainly by $\mathcal{E}$) and a magnetic-primary coherence control ($\tau_g^*, N_0$ governed mainly by $\mathcal{M}$). The paper closes with discriminating laboratory protocols, expressed entirely in QMU variables, that can determine which channel dominates coherence maintenance and threshold in valence-seat filling.

**Keywords:** QMU; APM; photoelectric effect; coherence window; gate quantization; holonomy

# 1 Introduction

Institutional attribution follows the QADI reference identity Thomson III [2025]. The photoelectric effect historically motivated the quantum hypothesis and its energy–frequency scaling in early work by Einstein Einstein [1905] and subsequent precision studies Millikan [1916]. Thermal rounding of threshold curves and near-threshold response are also well characterized in the Fowler framework Fowler [1931] and in photocathode phenomenology Spicer [1958].

Within the Aether Physics Model (APM) and Quantum Measurement Units (QMU), a prior foundation paper developed a gate interpretation Thomson III [2026] in which (i) photon fronts carry a fixed quantum phtn and (ii) intensity primarily controls event rate rather than per-event energetic payload. A remaining open thread is how to map the experimentally inferred post-threshold "stopping" descriptor to a fixed-quantum ontology without reintroducing a continuously variable photon quantum.

This note supplies that missing mapping using a single additional primitive: a finite *coherence window* $\tau_g$ for the valence-seat gate. The coherence window translates the photon-front cadence into an integer count of quanta that can be coherently accumulated into one emission event. The result is an event-level *staircase* law that can average to a quasi-linear trend in frequency ratio while remaining strictly quantized in the single-emitter limit. Operationally, the surplus $\mathrm{enrg}_e$ is the emitted-electron kinetic-energy descriptor (up to experimental broadening), while $N_0$ sets the threshold intercept.

Two further aims guide the presentation. First, the paper is written to permit both electrostatic and magnetic interpretations of valence-seat filling: the seat may be filled by mass strings (magnetic-channel bookkeeping) even if the laboratory suppression readout is implemented by electrode bias (electrostatic-channel bookkeeping). Second, the two perspectives are made experimentally separable by assigning the coherence-control variables $(\tau_g^*, N_0)$ to either an electrostatic control state $\mathcal{E}$ or a magnetic control state $\mathcal{M}$, and by providing decision criteria based on sensitivity ratios.

Sections 2–3 define $\tau_g$ and derive $N(\nu^*)$; Section 4 states the dual $(\varphi_e, \psi_e)$ parametrization and

E/M control hypotheses; Section 5 lists discriminating protocols.

## 2 Ledger closure check

A canonical closure used for sanity checks is Ledger One,

$$A_u \,\mathrm{curl} = {F_q}^2 \, {\lambda_C}^2.$$

With the propagation product $F_q \, \lambda_C$ recognized as the photon-speed constant in QMU bookkeeping, Ledger One is the QMU decomposition of the electromagnetic propagation constant into rotational (Aether unit) and torsional (curl) geometries.

## 3 Coherence window and integer-count kinematics

### 3.1 Dimensionless frequency ratio and gate window

Define the dimensionless frequency ratio

$$\nu^* \;:=\; \frac{\nu}{F_q}, \tag{1}$$

and define the gate coherence window $\tau_g$ with its dimensionless form

$$\tau_g^* \;:=\; \tau_g \, F_q. \tag{2}$$

Operationally, $\tau_g$ is the maximum interval over which a valence-seat configuration can remain phase-locked to incident photon fronts such that their fixed quanta can accumulate coherently into a single emission event.

### 3.2 Integer quantum count admitted per event

Within one coherence window, the number of photon-front opportunities is the cadence count $\nu \, \tau_g$. In dimensionless variables, this yields the integer admissible count

$$N(\nu^*) \;:=\; \lfloor \nu \, \tau_g \rfloor \;=\; \left\lfloor \nu^* \, \tau_g^* \right\rfloor, \tag{3}$$

where $\lfloor \cdot \rfloor$ denotes the floor function. The coherence window thus converts a continuous scan of $\nu^*$ into a stepwise increasing integer $N$.

### 3.3 Threshold count

Introduce an integer threshold $N_0$ that encodes the minimum count required to complete valence-seat filling, release an electron, or otherwise open the emission gate:

$$\text{gate opens} \quad \Longleftrightarrow \quad N(\nu^*) \geq N_0. \tag{4}$$

This condition is the integer-count refinement of the binary gate state used in the foundation paper: the earlier $\mathcal{G} \in \{0, 1\}$ "gate open" indicator corresponds here to $\mathcal{G} = 1$ if and only if $N(\nu^*) \geq N_0$. In laboratory observations, $N_0$ is what appears as a threshold frequency ratio $\nu_{\mathrm{th}}^*$, subject to thermal rounding and surface preparation effects Fowler [1931], Spicer [1958].

# 4 Event energy surplus law

## 4.1 Fixed-quantum surplus

Let phtn denote the fixed photon quantum in QMU bookkeeping and let $\mathrm{enrg}_e(\nu^*)$ denote the event energy delivered to the escaping electron state (or to the emission channel more broadly). Define a coupling efficiency $\eta \in (0, 1]$ that aggregates alignment and gate-capture probability during the coherence window. Then the simplest integer surplus law consistent with Eqs. (3) and (4) is

$$\mathrm{enrg}_e(\nu^*) \;:=\; \eta\,\big(N(\nu^*) - N_0\big)_+ \,\mathrm{phtn}, \qquad (x)_+ := \max(x, 0). \tag{5}$$

In the limit of negligible thermal smear and negligible post-emission scattering, $\mathrm{enrg}_e$ may be identified directly with the maximum kinetic energy of the emitted electron for that configuration (the quantity conventionally plotted as $K_{\max}$ in the Einstein form $K_{\max} = h\nu - \Phi$). Here, the role of $h\nu$ is replaced by the cadence-count surplus over a finite coherence window, while the threshold is encoded by the integer $N_0$. The law has three direct consequences.

**(i) Threshold.** For $N < N_0$, the event energy vanishes and emission is forbidden by the gate condition.

**(ii) Staircase post-threshold scaling.** For $N \geq N_0$, the event energy increases in discrete steps of size $\eta\,\mathrm{phtn}$ whenever $N$ increments.

**(iii) Quasi-linear large-count envelope.** For $\nu^*\,\tau_g^* \gg 1$, the staircase has an envelope

$$\mathrm{enrg}_e(\nu^*) \;\approx\; \eta\,\big(\nu^*\,\tau_g^* - N_0\big)\,\mathrm{phtn}, \tag{6}$$

with residual oscillation bounded by one quantum step due to the floor operation. Under ensemble averaging (many sites, drifting micro-geometry, or moderate thermal smear), the staircase tends to a smooth curve, which is how a quasi-linear frequency dependence can appear experimentally without assigning a continuously variable quantum to a single photon front.

## 4.2 Step spacing in frequency ratio

Because $N$ increments by one when $\nu^*\,\tau_g^*$ crosses an integer, the characteristic step spacing in $\nu^*$ is

$$\Delta\nu^* \;=\; \frac{1}{\tau_g^*}. \tag{7}$$

Thus, extracting $\Delta\nu^*$ from high-resolution single-emitter data provides a direct measurement of the dimensionless coherence window $\tau_g^*$. For the optional topology-set value $\tau_g^* = 16\pi^3$ in Eq. (17), the spacing is $\Delta\nu^* \approx 1/496$; in standard macroscopic measurements the combination of site-to-site variation, thermal rounding, and instrumental bandwidth makes this spacing effectively a continuum, which explains why the staircase structure is not typically visible without single-emitter isolation.

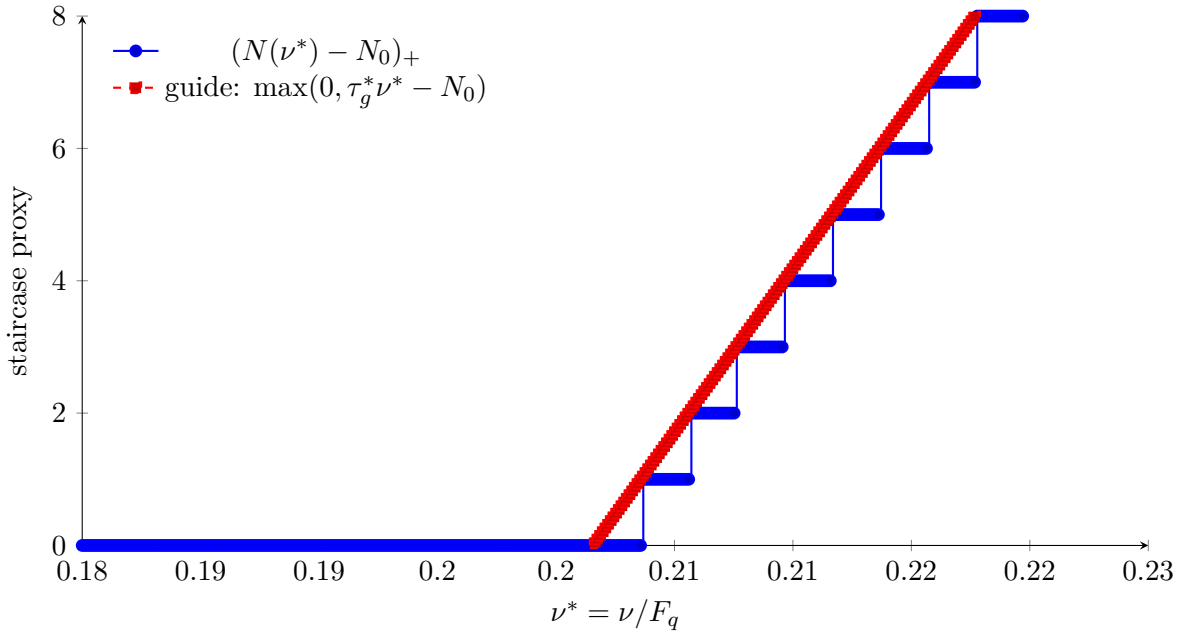


Figure 1: Coherence-window quantization produces a staircase in $\nu^*$. The plotted proxy is $(N(\nu^*) - N_0)_+$ with $N(\nu^*) = \lfloor \nu^* \tau_g^* \rfloor$. Ensemble averaging (site-to-site variation, thermal smear, or mild jitter in $\tau_g^*$ and alignment) smooths the micro-steps toward the dashed envelope.

### 4.3 Worked example: threshold and one-step increments in $\nu^*$

Choose a representative coherence window and threshold count:

$$\tau_g^* = 16\pi^3 \approx 4.961 \times 10^2, \qquad N_0 = 100, \qquad \eta = 1.$$

The quantum-count function $N(\nu^*) = \lfloor \nu^* \tau_g^* \rfloor$ implies a step spacing

$$\Delta\nu^* = \frac{1}{\tau_g^*} \approx 2.016 \times 10^{-3},$$

and a threshold frequency ratio

$$\nu_{\text{th}}^* \approx \frac{N_0}{\tau_g^*} \approx 2.016 \times 10^{-1}.$$

Now evaluate three nearby points.

**(i) Below threshold.** Let $\nu_1^* = 0.2010$. Then $N(\nu_1^*) = \lfloor 0.2010\, \tau_g^* \rfloor = \lfloor 99.7 \rfloor = 99 < N_0$ and

$$\text{enrg}_e(\nu_1^*) = \eta\, (N - N_0)_+ \,\text{phtn} = 0.$$

**(ii) At threshold integer.** Let $\nu_2^* = 0.2020$. Then $N(\nu_2^*) = \lfloor 0.2020\, \tau_g^* \rfloor = \lfloor 100.2 \rfloor = 100$ and

$$\text{enrg}_e(\nu_2^*) = 0 \cdot \text{phtn},$$

so the first admissible integer $N = N_0$ corresponds to gate opening without surplus.

**(iii) Next step.** Let $\nu_3^* = \nu_2^* + \Delta\nu^* \approx 0.2040$. Then $N(\nu_3^*) = 101$ and the event surplus is one quantum:

$$\mathrm{enrg}_e(\nu_3^*) = 1 \cdot \mathrm{phtn}.$$

The same event energy can be expressed in either charge channel:

$$\varphi_e(\nu_3^*) = \frac{\mathrm{phtn}}{e^2}, \qquad \psi_e(\nu_3^*) = \frac{\mathrm{phtn}}{{e_{\mathrm{emax}}}^2}, \qquad \psi_e = (8\pi\alpha)\,\varphi_e,$$

using ${e_{\mathrm{emax}}}^2 = e^2/(8\pi\alpha)$.

# 5 Dual-channel stopping descriptors

## 5.1 Electrostatic and magnetic conjugate scalars

To preserve both electrostatic and magnetic interpretations in a testable way, we introduce two conjugate potential-like scalars that parameterize the same event energy Eq. (5) in different QMU charge primitives:

$$\varphi_e(\nu^*) \;:=\; \frac{\mathrm{enrg}_e(\nu^*)}{e^2}, \qquad \psi_e(\nu^*) \;:=\; \frac{\mathrm{enrg}_e(\nu^*)}{{e_{\mathrm{emax}}}^2}. \tag{8}$$

In an electrode-bias stopping experiment, the laboratory readout is naturally expressed as an electrostatic barrier scale (hence $\varphi_e$). In a valence-seat filling interpretation where mass strings dominate the internal gate energetics, the native bookkeeping may be magnetic-channel (hence $\psi_e$).

Because the QMU primitives are related by

$${e_{\mathrm{emax}}}^2 \;=\; \frac{e^2}{8\pi\alpha}, \tag{9}$$

the two descriptors are exactly convertible:

$$\psi_e \;=\; (8\pi\alpha)\,\varphi_e. \tag{10}$$

Therefore, the distinction between "electrostatic stop" and "magnetic stop" is *not* a dispute about the measured event energy. It is a dispute about which channel dominantly controls the gate variables $(\tau_g^*, N_0, \eta)$.

## 5.2 Staircase law in either channel

Substituting Eq. (5) into Eq. (8) yields

$$\varphi_e(\nu^*) \;=\; \eta\,\big(N(\nu^*) - N_0\big)_+\,\frac{\mathrm{phtn}}{e^2}, \tag{11}$$

and

$$\psi_e(\nu^*) \;=\; \eta\,\big(N(\nu^*) - N_0\big)_+\,\frac{\mathrm{phtn}}{{e_{\mathrm{emax}}}^2}. \tag{12}$$

The step spacing in $\nu^*$ is identical in both plots; the vertical scaling differs only by the constant factor Eq. (10).

# 6 Two competing gate laws

The coherence-window mechanism by itself does not choose which physical boundary channel controls $\tau_g^*$ and $N_0$. We therefore define two competing, experimentally separable gate laws.

## 6.1 Electrostatic-primary gate law (E-gate)

Let $\mathcal{E}$ denote an electrostatic control state of the emitter environment: electrode bias geometry, surface charge preparation, and field shaping proximate to the emission site. The electrostatic-primary hypothesis is

$$\tau_g^* = \tau_g^*(\mathcal{E}), \qquad N_0 = N_0(\mathcal{E}), \qquad \eta = \eta(\mathcal{E}, \text{alignment}). \tag{13}$$

In words: the gate remains coherent, and reaches threshold, primarily through electrostatic organization of the Aether-unit environment. Magnetic environment changes act secondarily (e.g., mainly by altering trajectory collection rather than the gate itself).

## 6.2 Magnetic-primary gate law (M-gate)

Let $\mathcal{M}$ denote a magnetic control state: static guiding fields, shielding, loop-closure geometry, and orientation relative to the holonomy axis of the Aether unit. The magnetic-primary hypothesis is

$$\tau_g^* = \tau_g^*(\mathcal{M}), \qquad N_0 = N_0(\mathcal{M}), \qquad \eta = \eta(\mathcal{M}, \text{alignment}). \tag{14}$$

In words: valence-seat filling is controlled by mass-string accumulation, so coherence maintenance and threshold are primarily magnetic-channel. Electrostatic controls matter chiefly as readout barriers and as secondary organizers of boundary conditions.

## 6.3 What differs observationally

Both hypotheses predict the same staircase form Eqs. (11) and (12). The discriminator is which controlled knob moves the two structurally diagnostic quantities:

- step spacing $\Delta\nu^* = 1/\tau_g^*$ (coherence window), and
- threshold position (encoded by $N_0$ or by $\nu_{\text{th}}^*$).

A change that mainly affects collection efficiency will mostly change $\eta$ and the event rate, but it should not move $\Delta\nu^*$ in a single-emitter regime. A change that affects the gate coherence will move $\Delta\nu^*$ through $\tau_g^*$.

# 7 Discriminating experiments in QMU form

This section states protocols entirely in dimensionless variables. The aim is to extract $\tau_g^*$ and $N_0$ from data, then compare their sensitivity to independent electrostatic and magnetic control perturbations.

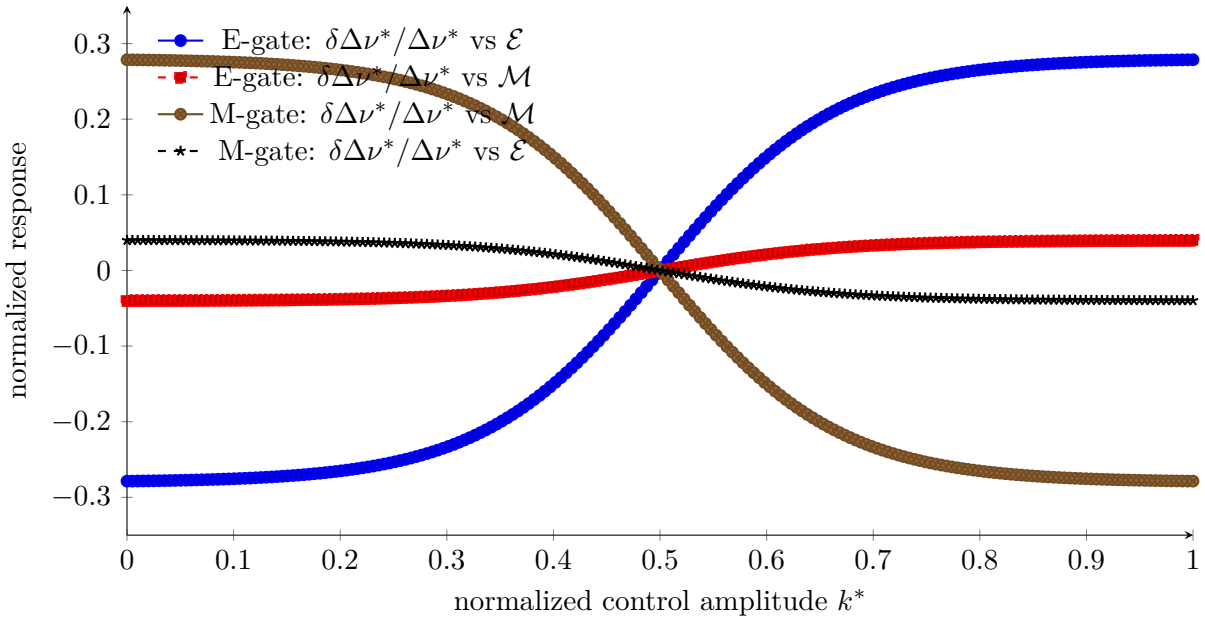


Figure 2: Schematic knob-sensitivity discriminator for the coherence spacing. The measured step spacing is $\Delta\nu^* = 1/\tau_g^*$. Under the electrostatic-primary hypothesis (E-gate), $\Delta\nu^*$ responds strongly to changes in $\mathcal{E}$ and weakly to changes in $\mathcal{M}$; under the magnetic-primary hypothesis (M-gate) the roles reverse. The experimental decision is made by comparing the extracted sensitivity ratio $\mathcal{R}_\tau$ in Eq. (15), not by the specific functional form shown here.

### 7.1 Protocol A: step-spacing sensitivity

Work in a regime as close as possible to single-emitter behavior so that the staircase contrast is preserved. Measure $\varphi_e(\nu^*)$ (electrode-defined readout) or equivalently $\psi_e(\nu^*)$ (magnetic parameterization). From the micro-step pattern, extract $\Delta\nu^*$ and thus $\tau_g^*$ via Eq. (7).

Now apply two perturbations:

1. **Electrostatic perturbation** $\Delta\mathcal{E}$ at fixed $\mathcal{M}$ (e.g., modify bias geometry or near-field shaping without changing external magnetic configuration).
2. **Magnetic perturbation** $\Delta\mathcal{M}$ at fixed $\mathcal{E}$ (e.g., add shielding or a static guiding field, or rotate the emitter relative to the field).

Compute the sensitivity ratio

$$\mathcal{R}_\tau := \frac{|\partial\Delta\nu^*/\partial\mathcal{E}|}{|\partial\Delta\nu^*/\partial\mathcal{M}|} = \frac{\left|\partial(1/\tau_g^*)/\partial\mathcal{E}\right|}{\left|\partial(1/\tau_g^*)/\partial\mathcal{M}\right|}. \tag{15}$$

Decision rule: $\mathcal{R}_\tau \gg 1$ favors E-gate, while $\mathcal{R}_\tau \ll 1$ favors M-gate. An intermediate value indicates mixed control.

### 7.2 Protocol B: threshold sensitivity

Extract a threshold frequency ratio $\nu^*_{\mathrm{th}}$ from the onset of nonzero events, or equivalently infer $N_0$ by locating the first sustained step in $N(\nu^*)$ consistent with Eq. (4). Repeat the same two perturbations and compute

$$\mathcal{R}_0 \;:=\; \frac{|\partial N_0/\partial \mathcal{E}|}{|\partial N_0/\partial \mathcal{M}|}. \tag{16}$$

Decision rule: $\mathcal{R}_0 \gg 1$ favors E-gate, while $\mathcal{R}_0 \ll 1$ favors M-gate.

### 7.3 Protocol C: disentangling $\eta$ from coherence

To avoid mis-attribution, include an alignment/polarization scan at fixed $\mathcal{E}, \mathcal{M}$. If the primary effect is a change in staircase *contrast* (step heights, event probability), the change is captured by $\eta$. If the primary effect is a change in *spacing* or threshold position, the change must enter through $\tau_g^*$ and/or $N_0$.

### 7.4 Protocol D: mixed-frequency driving

Illuminate with two discrete frequency ratios $\nu_1^*$ and $\nu_2^*$ under otherwise fixed conditions. If coherence accumulation is operative, then within one $\tau_g^*$ window the admitted count can include integer combinations. This predicts secondary structure in the event descriptors that depends on $\lfloor \nu_1^* \tau_g^* \rfloor + \lfloor \nu_2^* \tau_g^* \rfloor$ rather than only on the weighted mean frequency. Such combination signatures help distinguish cadence-counting from any model in which per-event energy is set by a single instantaneous frequency alone.

## 8 Discussion

The coherence-window primitive $\tau_g^*$ is the only new ingredient required to obtain a quantized event-level mapping from fixed photon quanta to post-threshold energetic descriptors. The quantization is strict in the single-emitter limit (staircase), but it naturally smooths under ensemble averaging, providing a route to quasi-linear frequency trends without assigning a continuously variable quantum to a single photon front.

The electrostatic versus magnetic debate is therefore re-framed into a clean empirical question: *which boundary channel dominantly controls coherence maintenance and threshold*? Because the readout can be expressed in either conjugate scalar via Eq. (10), the decisive evidence must come from the sensitivity ratios Eqs. (15) and (16) rather than from the choice of vertical axis. In the APM valence-seat interpretation, it is plausible that $N_0$ is primarily magnetic (mass-string filling), while the laboratory suppression is electrostatic (electrode barrier). The protocols above allow that mixed case to be recognized rather than forced into a single-channel narrative.

Finally, temperature and surface preparation effects (captured empirically in conventional literature by threshold rounding and distribution functions Fowler [1931], Spicer [1958]) can be absorbed here as broadenings of the effective coherence window and as site-to-site fluctuations in $N_0$ and $\eta$. This is a useful translation layer: it allows existing datasets to be reanalyzed in QMU variables by extracting $\tau_g^*$ and $N_0$ distributions rather than fitting continuous-energy emission models.

## 9 Conclusion

A coherence window $\tau_g^*$ converts fixed-quantum photon-front cadence into an integer-count gate law for photoemission events. The resulting surplus law yields a threshold and a quantized staircase post-threshold descriptor with step spacing $\Delta\nu^* = 1/\tau_g^*$, while preserving quasi-linear trends under averaging. By introducing dual conjugate stopping descriptors $(\varphi_e, \psi_e)$ and by stating two competing gate laws (E-gate and M-gate), the framework enables direct laboratory discrimination of electrostatic versus magnetic dominance in coherence control and valence-seat filling.

## A Optional topology-set closure for the coherence window

A separate holonomy-index note proposes a topology-set polarization rotation angle $\beta_0 = 1/(16\pi^2)$ per minimal-cell boundary traversal Thomson and Bourassa [2025]. If the gate coherence is limited by cumulative holonomy slip at a fixed increment per chronovibrational tick, a parameter-free candidate coherence window follows from a dephasing criterion such as $\beta_0\,\tau_g^* = \pi$:

$$\tau_g^* \;=\; \frac{\pi}{\beta_0} \;=\; 16\pi^3, \qquad \Delta\nu^* \;=\; \frac{1}{16\pi^3}. \tag{17}$$

This closure is optional: the main results of the paper require only that $\tau_g^*$ exists and can be extracted from data. If Eq. (17) holds, it predicts a universal step spacing in $\nu^*$ under sufficiently clean single-emitter conditions; departures then quantify how material-specific boundary conditions perturb the holonomy slip rate.

## Acknowledgments

The Quantum AetherDynamics Institute (QADI) is a private 501(c)(3) research institute developing the Aether Physics Model (APM) and Quantum Measurement Units (QMU). Publications and data are archived with DOIs in the AetherPhysics Zenodo community: zenodo.org/communities/aetherphysics.

## References

Albert Einstein. Über einen die erzeugung und verwandlung des lichtes betreffenden heuristischen gesichtspunkt. *Annalen der Physik*, 322(6):132–148, 1905. doi: 10.1002/andp.19053220607. URL https://doi.org/10.1002/andp.19053220607.

R. H. Fowler. The analysis of photoelectric sensitivity curves for clean metals at various temperatures. *Physical Review*, 38(1):45–56, 1931. doi: 10.1103/PhysRev.38.45. URL https://doi.org/10.1103/PhysRev.38.45.

Robert A. Millikan. Einstein's photoelectric equation and contact electromotive force. *Physical Review*, 7(1):18–32, 1916. doi: 10.1103/PhysRev.7.18. URL https://doi.org/10.1103/PhysRev.7.18.

W. E. Spicer. Photoemissive, photoconductive, and optical absorption studies of alkali-antimony compounds. *Physical Review*, 112(1):114–122, 1958. doi: 10.1103/PhysRev.112.114. URL https://doi.org/10.1103/PhysRev.112.114.

David W. Thomson and James D. Bourassa. A topological origin for cosmic birefringence: A parameter-free prediction of $\beta_0 = 1/(16\pi^2)$. Zenodo, September 2025. URL https://doi.org/10.5281/zenodo.17069938.

David W. Thomson III. Quantum aetherdynamics institute (qadi): Community doi overview and citation guide. Zenodo, 2025. URL https://doi.org/10.5281/zenodo.17479314.

David W. Thomson III. Aether-unit mechanism for the photoelectric effect (qmu/qadi: Ledger one transport, holonomy-projected photon geometry, and resonance gating). Zenodo, 2026. URL https://doi.org/10.5281/zenodo.18392964.